

1 U.S. NO₂ trends (2005–2013): EPA Air Quality System
2 (AQS) data versus improved observations from the
3 Ozone Monitoring Instrument (OMI)

4 Lok N. Lamsal^{a,b,*}, Bryan N. Duncan^b, Yasuko Yoshida^{c,b}, Nickolay A.
5 Krotkov^b, Kenneth E. Pickering^b, David G. Streets^d, Zifeng Lu^d

6 ^a*Goddard Earth Sciences Technology and Research, Universities Space Research
7 Association, Columbia, MD, USA*

8 ^b*NASA Goddard Space Flight Center, Greenbelt, MD, USA*

9 ^c*Science Systems and Applications, Inc., MD, USA*

10 ^d*Decision and Information Sciences Division, Argonne National Laboratory, Argonne,
11 IL, USA*

12 **Abstract**

13 Emissions of nitrogen oxides (NO_x) and, subsequently, atmospheric levels
14 of nitrogen dioxide (NO₂) have decreased over the U.S. due to a combination
15 of environmental policies and technological change. Consequently, NO₂ levels
16 have decreased by 30–40% in the last decade. We quantify NO₂ trends (2005–
17 2013) over the U.S. using surface measurements from the U.S. Environmental
18 Protection Agency (EPA) Air Quality System (AQS) and an improved tro-
19 pospheric NO₂ vertical column density (VCD) data product from the Ozone
20 Monitoring Instrument (OMI) on the Aura satellite. We demonstrate that
21 the current OMI NO₂ algorithm is of sufficient maturity to allow a favorable
22 correspondence of trends and variations in OMI and AQS data. Our trend
23 model accounts for the non-linear dependence of the NO₂ concentration on
24 emissions associated with the seasonal variation of the chemical lifetime, in-
25 cluding the change in the amplitude of the seasonal cycle associated with

*Corresponding author
Preprint submitted to Atmospheric Environment
Email address: lok.lamsal@nasa.gov (Lok N. Lamsal)

February 2, 2015

26 the significant change in NO_x emissions that occurred over the last decade.
27 The direct relationship between observations and emissions becomes more
28 robust when one accounts for these non-linear dependencies. We improve
29 the OMI NO_2 standard retrieval algorithm and, subsequently, the data prod-
30 uct by using monthly vertical concentration profiles, a required algorithm
31 input, from a high-resolution chemistry and transport model (CTM) sim-
32 ulation with varying emissions (2005–2013). The impact of neglecting the
33 time-dependence of the profiles leads to errors in trend estimation, particu-
34 larly in regions where emissions have changed substantially. For example, we
35 find that by including the time-dependency there are 18% more instances of
36 significant trends and up to 15% larger total NO_2 reduction. Using a CTM,
37 we explore the theoretical relation of the trends estimated from NO_2 VCDs
38 to those estimated from ground-level concentrations. The model-simulated
39 trends in VCDs strongly correlate with those estimated from surface concen-
40 trations ($r = 0.83$, $N = 355$). We then explore the observed correspondence
41 of trends estimated from OMI and AQS data. We find a significant, but
42 slightly weaker, correspondence (i.e., $r = 0.68$, $N = 208$) than predicted by
43 the model and discuss some of the important factors affecting the relation-
44 ship, including known problems (e.g., NO_z interferences) associated with the
45 AQS data. This significant correspondence gives confidence in trend and
46 surface concentration estimates from OMI VCDs for locations, such as the
47 majority of the U.S. and globe, that are not covered by surface monitoring
48 networks. Using our improved trend model and our enhanced OMI data
49 product, we find that both OMI and AQS data show substantial downward
50 trends from 2005 to 2013, with an average reduction of 38% for each over

51 the U.S. The annual reduction rates inferred from OMI and AQS measure-
52 ments are larger (-5.0%/yr, -3.7%/yr) from 2005 to 2008 than 2010 to 2013
53 (-1.6%/yr, -2.8%/yr). We quantify NO₂ trends for major U.S. cities and
54 power plants; the latter suggest the largest trend (-4%/yr) by 2008 and
55 small or insignificant changes during 2010–2013.

56 *Keywords:* Nitrogen dioxide, troposphere, air quality, trend, Aura OMI

57 **1. Introduction**

58 Emissions of nitrogen oxides (NO_x = NO + NO₂) are regulated by the
59 U.S. Environmental Protection Agency (EPA), because NO_x contributes to
60 the formation of unhealthy levels of surface ozone, a pollutant that has been
61 long known to damage lung tissue when inhaled (Kleinfield et al., 1957;
62 Challen et al., 1958). Though nitrogen dioxide (NO₂) is a respiratory ir-
63 ritant, its levels in the U.S. are currently below the National Ambient Air
64 Quality Standard (NAAQS) set by EPA (EPA, 2008). As a result of emis-
65 sion reductions from mobile and point sources (e.g., McDonald et al., 2012;
66 Xing et al., 2013), surface NO₂ levels in the U.S. decreased by 33% between
67 2001 and 2010 and, subsequently, ozone concentrations decreased by 14%,
68 when year-to-year variations in meteorology are taken into account (EPA,
69 2012). The temporal evolution of this substantial decrease in NO₂ has been
70 recorded by the Ozone Monitoring Instrument (OMI), which was launched on
71 the NASA Aura satellite in July 2004 (Figure 1). In this manuscript, we show
72 that recent modifications to the OMI retrieval algorithm have sufficiently im-
73 proved the quality of the data product so that trends and variations derived
74 from OMI and EPA Air Quality System (AQS) surface data are similar for

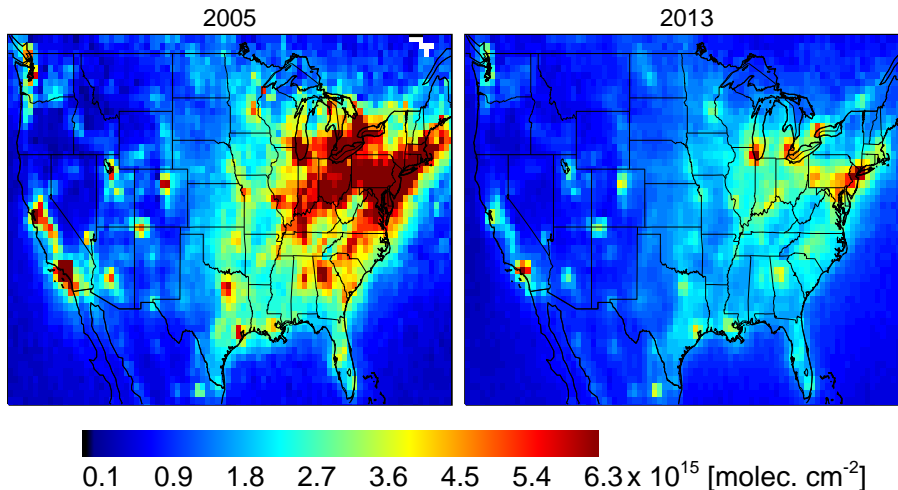


Figure 1: Annual average OMI tropospheric NO₂ VCDs at 1/2° latitude × 2/3° longitude spatial resolution for 2005 (left) and 2013 (right).

75 U.S. cities.

76 Tropospheric vertical column density (VCD) data of NO₂, as measured
 77 from space, serve as an effective proxy for surface NO₂ in many air quality
 78 applications. (The VCD is defined as the number of molecules of an at-
 79 mospheric gas between the satellite instrument and the Earth’s surface per
 80 unit area.) For instance, VCD data are used for inferring surface NO_x emis-
 81 sions (Leue et al., 2001; Martin et al., 2003; Jaeglé et al., 2005; Wang et al.,
 82 2007; Boersma et al., 2008a; Napelenok et al., 2008; Zhao and Wang, 2009;
 83 Lin et al., 2010; Lamsal et al., 2011; Streets et al., 2013; Tang et al., 2013;
 84 Ghude et al., 2013; Vinken et al., 2014), estimating trends and variations
 85 in atmospheric concentrations (Beirle et al., 2003; Richter et al., 2005; Frost
 86 et al., 2006; Boersma et al., 2008b; Lin and McElroy, 2011; Zhou et al., 2012;
 87 Castellanos and Boersma, 2012; Russell et al., 2012), monitoring emission
 88 changes in point sources (e.g., Kim et al., 2006; Wang et al., 2012; Duncan

89 et al., 2013), and inferring ozone formation sensitivities to NO_x and VOCs
90 levels (Martin et al., 2004; Duncan et al., 2010; Valin et al., 2013; Tang et al.,
91 2014). Duncan et al. (2013) demonstrated that variations and trends in OMI
92 NO_2 data near US power plants correlate well with changes in emissions re-
93 ported by the Continuous Emissions Monitoring System (CEMS) for large
94 facilities, particularly if they are located away from cities. Lamsal et al.
95 (2008, 2010) used an early version of OMI NO_2 data to infer ground-level
96 concentrations, such as those measured by the EPA AQS network, over a
97 range of locations and seasons. They found that their OMI-derived surface
98 concentrations, estimated using a chemistry and transport model (CTM),
99 were significantly correlated with AQS observations, both temporally and
100 spatially, though the correlations varied widely between monitoring stations.

101 The EPA AQS network of surface monitors is sparse and unevenly dis-
102 tributed, including in major metropolitan areas. The network lacks observa-
103 tions for large regions of the U.S. Because the lifetime of NO_x is short, trends
104 estimated from these monitoring data may not be spatially representative,
105 confounding NO_2 trend estimates derived from these surface data. Moreover,
106 NO_2 trends estimated from the commonly used chemiluminescent monitor
107 (equipped with molybdenum oxide converter) data may differ from true NO_2
108 trends because of interference from the oxidation products of NO_x (NO_z),
109 such as peroxyacetyl nitrate (PAN), alkyl nitrates, and nitric acid (HNO_3)
110 (Winer et al., 1974; Dunlea et al., 2007; Steinbacher et al., 2007; Lamsal
111 et al., 2008). Satellite observations, which have the advantage of spatial cov-
112 erage, provide information on NO_2 -specific trends, which complement and
113 enrich the AQS-observed trends. Here, we take advantage of three indepen-

114 dent measurements from OMI, a photolytic converter, and a molybdenum
115 converter to explore (1) how trends derived from OMI measurements, which
116 are collocated once per day, relate to trends available from high temporal res-
117 olution (hourly) surface data, and (2) how the interference in molybdenum
118 converter measurements could affect the actual observed NO₂ trend.

119 In this manuscript, we conduct a systematic investigation of the relation-
120 ship between AQS and OMI NO₂ trends; to our knowledge, such a trend
121 estimation and comparison have not been shown before. In Section 2, we de-
122 scribe our method for estimating trends, our new high-resolution OMI VCD
123 data product and the surface data that we use in our analysis. We also
124 present a model study of the expected correspondence of trends derived from
125 VCD and surface concentration data and discuss the various factors that
126 should be considered when comparing these trends. We discuss the observed
127 correspondence of trends derived from OMI VCD and AQS data in Section 3.
128 We summarize our conclusions in Section 4.

129 **2. Observations, model and methods**

130 *2.1. Multivariate linear regression for trend estimation*

131 We use a regression model to infer both the seasonal and the linear trend
132 components in OMI and AQS NO₂ observations. The time series of monthly
133 average NO₂ values (Ω) can be assumed to be comprised of three additive
134 subcomponents: a time dependent seasonal component (α), a linear trend
135 component (β), and residual or noise (R) component:

$$\Omega(t) = \alpha(t) + \beta(t) + R(t), \quad (1)$$

136 where t represents time (month). The time dependent regression component
137 (α) is given by a constant plus intra-annual sine and cosine harmonic series
138 (Randel and Cobb, 1994):

$$\alpha(t) = c_0 + \sum_{j=1}^3 (c_{1j} \sin(\frac{2\pi jt}{12}) + c_{2j} \cos(\frac{2\pi jt}{12})), \quad (2)$$

139 where c_0 , c_{1j} , and c_{2j} are constant coefficients to be determined from the
140 measurements. The major portion of the NO_2 annual cycle is explained by
141 the seasonal variation of the NO_x lifetime. The contributions from all other
142 factors, such as monthly variation in NO_x emissions, to the seasonal cycle
143 are typically small. The seasonal pattern may be constant or evolve in time.

144 Analysis of the temporal evolution of the seasonal variation of OMI NO_2
145 over the eastern U.S. reveals a considerable change (decrease) in seasonal
146 amplitude over the Aura record, suggesting the need of an approach that
147 accounts for it when calculating the trend and estimating trends in emis-
148 sions. Changes in the seasonal amplitude are also reported by Hilboll et al.
149 (2013) and occur at places where NO_x emissions are changing rapidly due to
150 economic growth or emission control measures. Removal of varying seasonal
151 components in a time series can be achieved by a locally weighted regression
152 smoothing technique (Cleveland et al., 1990) or by including a scaling factor
153 (Hilboll et al., 2013). In line with these methods, we identify and extract
154 seasonal and linear trend components by exploiting changes in the measured
155 seasonal pattern (amplitude and phase) for individual years. For each year,
156 Y , we fit a regression line using monthly observations from that year it-
157 self plus 6 monthly observations from years adjacent to Y . This provides a
158 series of local regression lines, which incorporate explicit time dependence.

159 Comparison of local regression lines with high- and low-amplitude regression
160 lines allows identification and isolation of two seasonal terms (α_1 , α_2 , where
161 $\alpha = \alpha_1 + \alpha_2$ in Eq. 1 and α_1 represents the regression line with the lowest
162 seasonal amplitude) and the linear trend (β). A graphical illustration of ap-
163 plying the multiple regression analysis to OMI data is shown in Figure A1
164 in AppendixA.

165 *2.2. The expected correspondence of NO₂ VCDs and surface concentrations*

166 As mentioned in Section 1, the primary advantage of satellite data for es-
167 timating trends is spatial coverage, especially for areas without surface mon-
168 itors or ones where the existing monitors do not provide NO₂ levels or trends
169 that are representative of an urban area as discussed in Section 2.4.3. In ad-
170 dition, a VCD has the advantage over surface data that it also includes NO₂
171 above the surface, which is necessary for estimating variations and trends
172 in NO_x levels and emissions from all sources, including power plants where
173 emissions are released well above the surface (i.e., tall smokestacks and plume
174 rise).

175 We use the NASA Global Modeling Initiative (GMI) CTM, which is de-
176 scribed in AppendixB, to examine how the trend in surface level NO₂ ob-
177 served by AQS relates to the trend in OMI VCD data. We examine the
178 observed correspondence in Section 3.1. The simulation includes annually
179 varying anthropogenic emissions and captures both the spatial distribution
180 and temporal changes observed by OMI over the continental U.S. (Strode
181 et al., 2014).

182 We apply the multivariate linear regression analysis, described in Sec-
183 tion 2.1, to the model output to calculate the linear trend component (β)

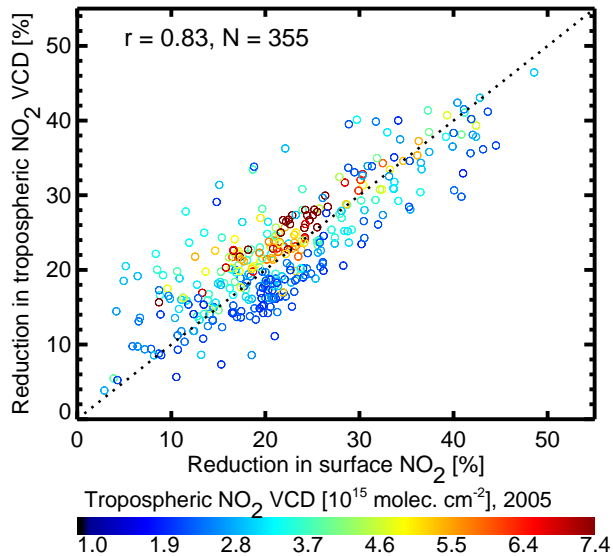


Figure 2: Model simulated reduction (% , 2005–2010) in surface NO_2 versus reduction in tropospheric NO_2 VCDs. Reductions in VCDs are color-coded by tropospheric NO_2 VCDs for 2005. The results are from a GMI simulation over the U.S., and include only areas with annual average tropospheric NO_2 VCDs $> 1 \times 10^{15}$ molecules cm^{-2} and statistically significant trends at the 95 % confidence level. The dotted line represents the 1:1 relationship.

184 in surface concentrations and tropospheric VCDs. Figure 2 compares the
 185 reductions (calculated from β) for 2005–2010 in surface NO_2 with those in
 186 tropospheric NO_2 VCDs over all polluted areas in the U.S. The trend in
 187 surface concentrations is well correlated ($r = 0.83$, $N = 355$) with the trend
 188 in VCDs, though, as expected, the scatter is higher for lower VCDs as the
 189 contribution of surface NO_2 to the tropospheric VCD is less than in polluted
 190 areas. The reductions in surface concentrations range from 6.4 to 42 %, while
 191 tropospheric VCD reductions range from 8.6 to 41 %. Reductions are higher
 192 over power plants in the tropospheric VCDs than the surface concentrations

193 because of tall smokestacks and plume rise associated with these sources.
194 The average reductions for the two quantities are in agreement to within
195 4%, but their correlation improves with increasing NO₂ levels (Figure 2).

196 *2.3. Description of OMI observations and recent improvements relevant for*
197 *U.S. air quality applications*

198 *2.3.1. Retrievals of tropospheric NO₂ VCD*

199 The OMI monitors NO₂ VCDs by measuring spectral variation in backscat-
200 tered solar radiation in the broad visible spectral window between 405 nm
201 and 465 nm. OMI measurements are made in early afternoon (i.e., local time
202 of 13:00–14:45) with a spatial resolution of 13 × 24 km² at nadir and with
203 nearly daily global coverage.

204 In this work, we further improve the operational OMI NO₂ retrieval algo-
205 rithm (NASA standard Product, version 2.1 see AppendixC), by using new a
206 priori NO₂ profiles simulated by the GMI CTM with year-specific emissions.
207 The profiles not only improve the representation of the NO₂ vertical distri-
208 bution, but also capture the yearly changes in NO₂ profile shapes. The latter
209 is critical due to rapid decline in the U.S. NO_x emissions in recent years (e.g.,
210 Figure 1), as NO₂ retrievals and, therefore, the estimated trends are sensitive
211 to the vertical shape of NO₂ profiles as discussed in Section 2.3.2.

212 We use individual pixel clear sky (cloud radiance fraction < 0.5) Level 2
213 OMI NO₂ data. The estimated errors in individual tropospheric NO₂ VCDs
214 observed under polluted (tropospheric NO₂ VCD > 1 × 10¹⁵ molecules cm⁻²)
215 and clear sky conditions are ~30% (Bucsela et al., 2013). To exclude the
216 cross-track rows affected by the row anomaly after 2007 and to avoid incon-
217 sistent sampling, we use OMI data for rows 5–23 for the entire OMI dataset.

218 The largest pixels that are at swath edges (rows 1–4) were excluded to reduce
219 spatial smearing of tropospheric NO₂. We then map the remaining data into
220 a 0.1° latitude × 0.1° longitude grid by calculating an area-weighted aver-
221 age. The approach accounts for the overlap and size of OMI ground footprints
222 (pixels). Finally, we compute monthly averages to estimate trends for the
223 entire OMI period (2005–2013).

224 *2.3.2. Impact on the OMI-derived trend of the assumption of the vertical*
225 *NO₂ distribution in the retrieval algorithm*

226 Satellite retrieval algorithms of NO₂ VCDs are sensitive to the assumed
227 vertical distribution of NO₂ (Martin et al., 2002; Boersma et al., 2004; Heckel
228 et al., 2011; Russell et al., 2011; Hains et al., 2010; Lamsal et al., 2014). Most
229 operational NO₂ retrieval algorithms assume an a priori vertical distribution,
230 such as those taken from a coarse-resolution CTM (e.g. Boersma et al., 2011;
231 Hilboll et al., 2013; Bucselá et al., 2013). Since the model simulations often
232 use outdated bottom-up emissions, these profiles may not capture the actual
233 vertical distribution of NO₂, especially where anthropogenic NO_x emissions
234 are undergoing rapid changes (e.g., Figure 1). For instance, the operational
235 OMI retrieval algorithm (NASA standard product, version 2.1) uses a cli-
236 matology of a priori NO₂ profiles at 2° latitude × 2.5° longitude horizontal
237 resolution from a GMI CTM simulation based on emissions from the 1999
238 National Emission Inventory (NEI). Here, we explore how the current prac-
239 tices of operational algorithms employing NO₂ profiles based on constant
240 and/or outdated emissions affect satellite-derived NO₂ trends.

241 As discussed in Section 2.3.1, we performed two separate retrievals, one
242 using monthly NO₂ vertical profiles based on emissions and meteorology of

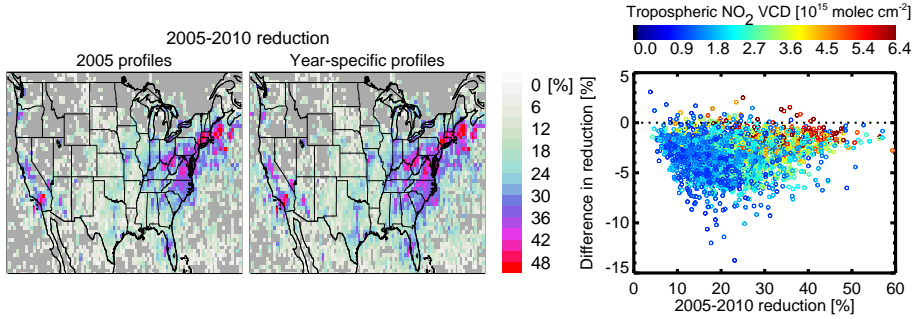


Figure 3: Percent reduction in OMI tropospheric NO_2 VCDs for 2005–2010 ($1/2^\circ$ latitude \times $2/3^\circ$ longitude horizontal resolution) calculated from two separate retrievals, one using 2005 (left) and another using year-specific (middle) monthly mean NO_2 vertical profiles. The dark gray color represents the locations with insignificant trends at 95 % confidence. (right) The difference between trends calculated from the retrievals based on 2005 profiles minus the retrievals based on year-specific profiles. Values are color-coded by average tropospheric NO_2 VCDs for 2005.

243 2005, which we refer to as “2005 profiles”, and another using monthly NO_2
 244 profiles based on year-specific emissions and meteorology, which we refer
 245 to as “year-specific profiles”, to demonstrate the impact of vertical profile
 246 assumptions on the OMI-derived NO_2 trends. Interannual variations in the
 247 meteorological fields are expected to have a minor effect on monthly average
 248 NO_2 data. We use OMI pixels with cloud radiance fraction < 0.5 , calculate
 249 area-weighted average VCDs on a $1/2^\circ$ latitude \times $2/3^\circ$ longitude horizontal
 250 grid, and use Eq. 1 to derive linear trends for 2005–2010.

251 Figure 3 shows the spatial variation of NO_2 reduction for 2005–2010 cal-
 252 culated from the two retrievals. Although the reductions from both retrievals
 253 are highly consistent with one another ($r = 0.97$, $N = 3524$), the year-specific
 254 retrievals offer a considerably higher number (18 %) of cases with significant

255 trends and up to 15 % larger reductions. Therefore, using 2005 profiles in
256 the retrievals underestimates the trends, on average, by 0.6 %/yr and overall
257 2005–2010 reduction by 3.5 %. The smaller deviations for larger VCDs imply
258 that the trend is less sensitive to the vertical profile assumption in highly
259 polluted areas. Since the vertical profiles used in the generation of OMI op-
260 erational products are based on NEI 1999, we anticipate that annual trends
261 estimated using these products would be biased low.

262 *2.4. Description of in situ surface NO₂ measurements and considerations for* 263 *trend estimation*

264 *2.4.1. AQS surface measurements*

265 We use hourly NO₂ measurements from the EPA AQS monitoring net-
266 work (Demerjian, 2000). The network employs the EPA-designated NO₂
267 chemiluminescence automated Federal Reference Method (FRM) described
268 in detail in EPA (1975). The NO₂ measurement method of these commercial
269 instruments relies on detecting NO by reducing NO₂ to NO on the surface of
270 a heated molybdenum oxide (MoO_x) substrate at 300–400°C. However, the
271 reduction of NO₂ to NO by the MoO_x substrate is not specific to NO₂, but is
272 also sensitive to some unknown fraction of NO_z (NO_z') (Winer et al., 1974;
273 Grosjean and Harrison, 1985; Demerjian, 2000; EPA, 2006; Dunlea et al.,
274 2007; Steinbacher et al., 2007; Lamsal et al., 2008). The magnitude of the
275 total interference is variable, and depends not only on the relative fraction of
276 actual NO₂ to total reactive nitrogen compounds (NO_y = NO_x + NO_z), but
277 also on the characteristics of individual monitors. As a result, NO₂ measure-
278 ments from AQS monitors are consistently biased high (up to 50 %), with
279 the highest biases in the afternoon as discussed in Section 2.4.2, at distant

280 locations from NO_x sources, and during summer months when these NO_z
281 products are expected to peak (e.g., Steinbacher et al., 2007). The Aura
282 overpass is once per day in early afternoon when this bias is near its daily
283 maximum.

284 To relate OMI with AQS observations, we select measurements collocated
285 in space and time. For overlapping OMI overpasses for a given day, we
286 compute averages weighted by OMI ground pixel sizes. The hourly data
287 from AQS are averaged over a 2-hour period (13:00–15:00 local time) to
288 temporally match with the OMI measurements. We exclude stations that
289 offer measurements only during the summer ozone season or ceased operation
290 anytime between 2005 and 2013. These criteria retain 208 sites, including
291 30 in rural, 89 in suburban, and 88 in urban environments. We also use the
292 hourly data from these sites to examine the diurnal variation in surface NO_2
293 trends in Section 4.

294 *2.4.2. Interferences in the AQS-observed trends*

295 Here we examine how the trend estimated from the biased AQS NO_2 data
296 relates to the actual NO_2 trend. We use hourly NO_2 observations made by
297 collocated MoO_x and more accurate photolytic converter instruments at a
298 rural site in Yorkville, Georgia, which is located 72 km to the northwest of
299 Atlanta. The photolytic converter instrument employs broadband photolysis
300 of ambient NO_2 followed by chemiluminescence detection of the product,
301 NO , offering a true NO_2 measurement with accuracy better than 10 % (Kley
302 and McFarland, 1980; Ryerson et al., 2000; Zellweger et al., 2000; Pollack
303 et al., 2010). Long-term photolytic converter measurements are available
304 from the SouthEastern Aerosol Research and Characterization (SEARCH)

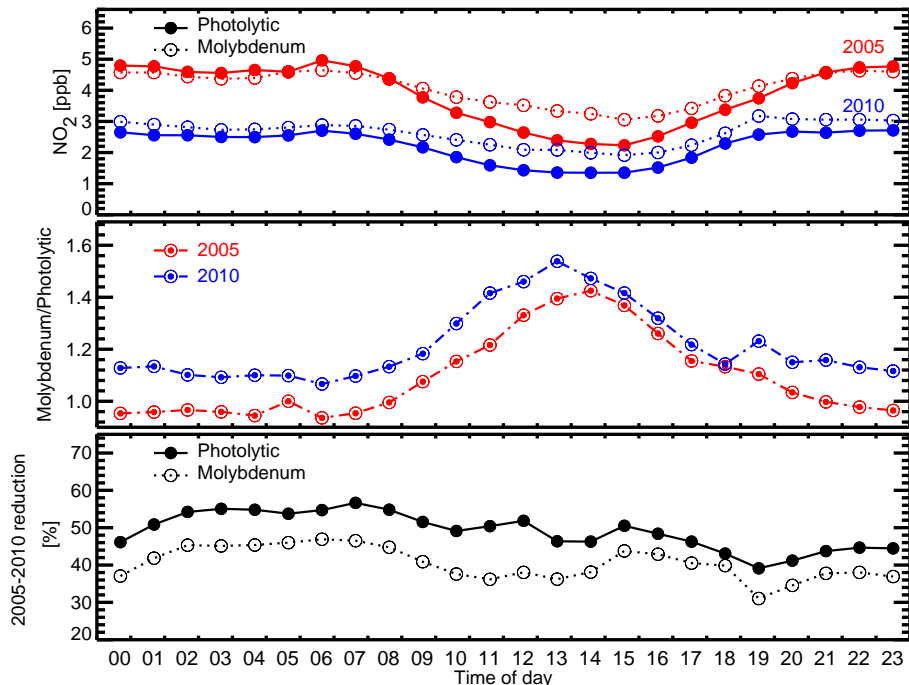


Figure 4: (top) Hourly averaged surface NO_2 mixing ratios for 2005 (red) and 2010 (blue) measured by collocated AQS molybdenum (dotted line open circles) and SEARCH photolytic (solid line with closed circles) converter analyzers at Yorkville, GA. (middle) Hourly variations of the ratio of the molybdenum and photolytic measurements for 2005 and 2010. (bottom) Diurnal changes in the NO_2 reductions for 2005–2010 calculated from the photolytic and molybdenum converter measurements.

305 network (Edgerton et al., 2006). We use the data for the period 2005–2010
 306 to calculate annual averages and monthly trends.

307 Figure 4 (top) shows the diurnal variation of annually averaged NO_2
 308 measured by the MoO_x converter and photolytic converter instruments. The
 309 two measurements agree to within 5% between 8 PM and 8 AM in 2005.
 310 Significant differences of 8–43% are observed during the day with the largest
 311 difference at 2–3 PM, near the OMI overpass time. The difference is a result

312 of the diurnal changes in the relative contribution of HNO₃, PAN, and alkyl
313 nitrates to NO_z' (Dunlea et al., 2007; Steinbacher et al., 2007; Lamsal et al.,
314 2008). In 2010, the biases increase, relative to 2005, not only in the early
315 and mid afternoon hours (22–54 %), but also in early morning (7–13 %) and
316 late afternoon (11–16 %), suggesting that the NO_z' interferences in the MoO_x
317 converter measurements have grown relative to NO₂ as NO₂ concentrations
318 have decreased in recent years. This result is not surprising given that the
319 formation of individual NO_z species is dependent on the NO_x concentration
320 (e.g., Duncan and Chameides, 1998). The bottom row of Figure 4 shows
321 NO₂ reductions for 2005–2010 calculated from the two datasets using the
322 same trend model (Eq. 1). Reductions in true NO₂ offered by the photolytic
323 converter measurements are on average 8.6 % higher than those calculated
324 from the molybdenum converter data.

325 The magnitude of NO_z', as well as the deviation of AQS-derived trends
326 from the actual NO₂ trends, are site specific and may not be identical to
327 the results from the case study presented here. They depend on several fac-
328 tors, including local meteorological conditions, speciation of local NO_z, the
329 distance between the site and emission sources (i.e., the degree of photo-
330 chemical aging), and characteristics of individual monitors. As a result, the
331 AQS-derived trends may differ from the actual NO₂ trends by a variable and
332 non-negligible amount. In fact, the results shown in Figure 4 imply that any
333 trend derived from AQS data would include a spurious trend introduced as
334 the NO₂ to NO_z' ratio changes over time with NO_x emission reductions. We
335 anticipate that impact of the NO_z' interferences will be less for AQS monitors
336 at highly polluted sites, where NO₂ makes up a larger fraction of NO_y, and

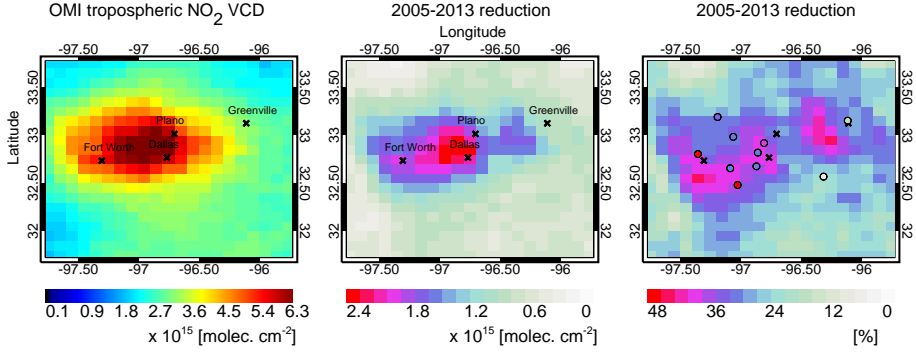


Figure 5: High resolution (0.1° latitude \times 0.1° longitude horizontal resolution) map of OMI tropospheric NO₂ VCDs for 2005 (left) and absolute (middle) and relative (right) reductions (derived from β in Eq. 1) in the VCDs for 2005–2013 over Dallas, TX. Crosses show the locations of four cities. Circles in the right panel show the percent reduction in NO₂ mixing ratios for 2005–2013 observed by the AQS monitors.

337 greater at background sites, where NO_z dominates.

338 *2.4.3. Spatial heterogeneity in NO₂ and implications for trends estimated*
 339 *from sparse surface stations*

340 There are obvious difficulties in relating local measurements from AQS
 341 with satellite observations. For instance, NO₂ is a short-lived species, so
 342 it is concentrated near combustion sources and, consequently, there can be
 343 considerable spatial heterogeneity in the NO₂ field near sources that is not
 344 resolved in the relatively spatially-coarse OMI measurements. Therefore, the
 345 AQS-derived NO₂ trends may reflect highly localized trends (e.g., near a
 346 highway) that cannot be captured in OMI trends. Thus, interpretation of
 347 the differences between the AQS- and OMI-derived trends at individual AQS
 348 sites is difficult, and is not expected to always show high correlations.

349 To illustrate this issue, we calculate trends using OMI data at 0.1° latitude

350 $\times 0.1^\circ$ longitude spatial resolution for Dallas, TX. Figure 5 shows the spatial
351 structure in the total decrease in OMI NO₂ levels from 2005 to 2013. In an
352 absolute sense, the largest decreases occurred where NO₂ levels are highest,
353 but in a relative sense, some of the largest changes are away from the city
354 center. For instance, there is a large relative decrease south of Fort Worth,
355 which is collocated with a major manufacturing area. Trends estimated from
356 the AQS monitors and OMI are similar at the majority of sites, but they ex-
357 hibit large discrepancies at some locations. These differences could arise from
358 preferential placement of monitors (e.g., next to highways), spatial variation
359 of source characteristics, and interference in surface NO₂ measurements as
360 discussed in Section 2.4.2. Therefore, trends derived from AQS data from
361 a specific city may not reflect area-wide average trends because the lack of
362 representativeness of those monitors (e.g., too few for a statistically signifi-
363 cant sample size). However, when averaged across all areas in this analysis,
364 we expect the trends to be robust as discussed in Section 3.

365 **3. Comparison between OMI and AQS trends over the Aura record** 366 **(2005–2013)**

367 In this section, we compare variations in the OMI tropospheric NO₂ VCDs
368 and AQS surface measurements, and explore the correspondence of trends
369 estimated from the two datasets.

370 *3.1. Trends for individual stations*

371 Figure 6 shows the annual average OMI tropospheric VCDs (at individual
372 AQS sites) and AQS surface mixing ratios for 2005 and 2013. Surface mea-
373 surements are sparse and unevenly distributed with most sites being located

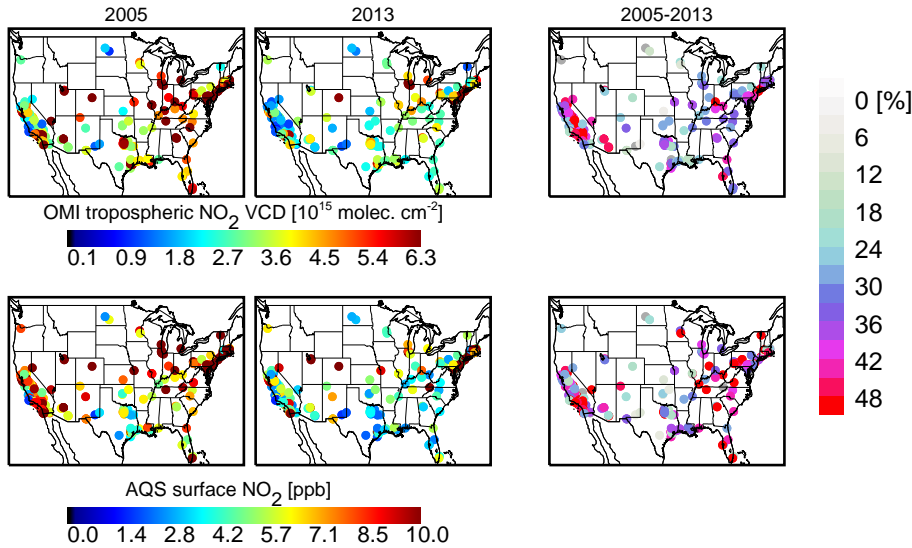


Figure 6: Collocated annually-averaged OMI tropospheric NO₂ VCDs (top row) and AQS surface (bottom row) concentrations for 2005 (left column) and 2013 (middle column). Total reduction (calculated from linear trend, β , in Eq. 1) from 2005 to 2013 (right column), where the gray color represents the locations with insignificant trends at 95% confidence.

374 in polluted regions. Both OMI and surface measurements exhibit broad simi-
 375 larities in both spatial distribution ($r = 0.76$, $N = 208$) and temporal changes.
 376 The total reductions from 2005 to 2013 (estimated from the linear trend, β)
 377 at individual sites generally range from 7.1% to 64% for OMI tropospheric
 378 NO₂ VCDs, and from 3.2% to 68% for AQS measurements. However, the
 379 average reductions at all sites are 38% for both the OMI and AQS datasets.
 380 As shown in Figure 7, the overall scatter is larger for the observed reductions
 381 in surface AQS data and VCDs as compared to what is predicted from the
 382 model simulation (Figure 2). This is not surprising given the measurement
 383 and sampling uncertainties that affect the trends derived from the OMI and
 384 AQS observations as discussed in Section 2. The correlation between the two

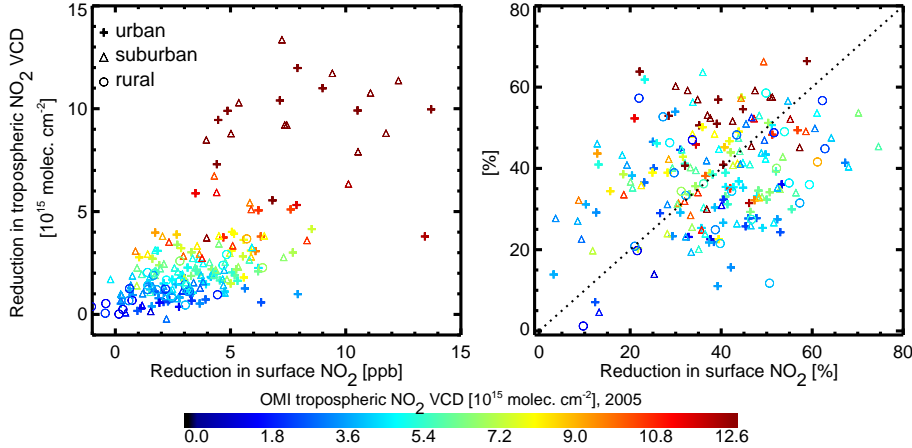


Figure 7: Scatter plot of the reductions derived from surface concentrations from individual AQS sites versus collocated OMI tropospheric VCDs in absolute values (left column) and percent (right column). Symbols indicate land use type: circles for urban, squares for suburban, and triangles for rural sites. Values are color coded by OMI tropospheric NO₂ VCDs for 2005. The dotted line represents the 1:1 relationship.

385 trends is significant ($r = 0.68$, $N = 208$).

386 *3.2. Trends by regions and EPA categories*

387 Tables 1–3 show comparisons of trends from OMI and AQS data grouped
 388 by regions, land type, and land use. Regional reductions from both datasets
 389 are in the range of 37–47%, with the largest reductions in southern Califor-
 390 nia (Table 1). In Tables 2 and 3, we compare the trend in OMI and AQS
 391 measurements according to EPA’s classification of the monitoring sites by
 392 land type and land use, respectively. Average reductions calculated from
 393 OMI and AQS measurements for all land uses and types range from 35%
 394 to 43%, and agree to within 3% with the exception of land type designated
 395 as mobile. Since there are few sites in this category and the classification

Table 1: Average Reduction by Regions.

Region	Domain	Number of sites	NO ₂ reduction (%)	
			AQS	OMI
New England	41–45°N, 70–75°W	13	38.3	37.9
Mid-Atlantic	36–41°N, 72–81°W	19	41.4	43.1
S. California	31–36°N, 116–122°W	50	42.8	47.2
Central Valley	36–41°N, 118–124°W	30	37.2	41.2

Table 2: Average Reduction at AQS Sites Grouped by Land Types.

Land type	Number of sites	NO ₂ reduction (%)	
		AQS	OMI
Mobile	6	34.9	43.1
Industrial	15	37.2	34.7
Agriculture	19	35.7	38.7
Commercial	74	39.5	37.0
Residential	88	37.9	40.3

Table 3: Average Reduction at AQS Sites Grouped by Land Uses.

Land use	Number of sites	NO ₂ reduction (%)	
		AQS	OMI
Rural	30	35.1	35.5
Suburban	89	39.0	40.1
Urban and center city	88	37.6	37.2

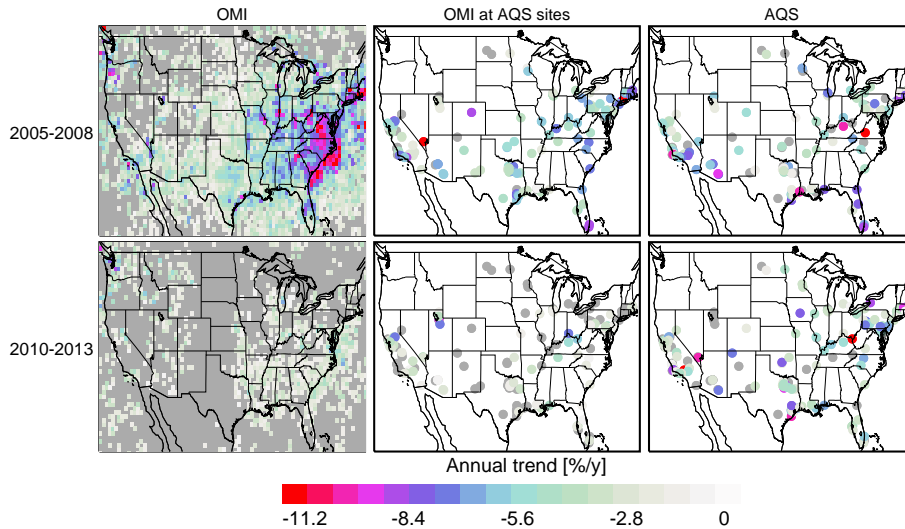


Figure 8: Annual trend (%/yr) for 2005–2008 (top row) and 2010–2013 (bottom row) for OMI data ($1/2^\circ$ latitude \times $2/3^\circ$ longitude horizontal resolution; left column), OMI data over AQS sites (middle column), and AQS data (right column). The dark gray color represents locations with insignificant trends at the 95 % confidence level.

396 does not provide information on local sources and their characteristics, it is
 397 difficult to interpret the somewhat larger difference.

398 3.3. Variations in the pace of NO_2 reductions

399 To examine variations in the pace of NO_2 reductions, we analyze the time
 400 series for β for two time periods, 2005–2008 and 2010–2013. The majority of
 401 the decrease in OMI NO_2 levels occurred in the earlier period with less of a
 402 decrease or even a slight increase in the latter period as discussed in Russell
 403 et al. (2012). Figure 8 shows the spatial variation of the annual trend in OMI
 404 tropospheric NO_2 VCDs for the 2005–2008 and 2010–2013 periods. There
 405 are significant decreasing trends over large areas of the U.S. during 2005–
 406 2008 with an annual reduction rate of 0–12 %. Reductions are more rapid

407 in many populated areas of the U.S.; trends in sparsely populated areas
408 are small or insignificant. The trends are substantially weaker during 2010–
409 2013. Figure 8 compares the trends observed by OMI and AQS monitors.
410 The spatial distribution as well as the magnitude of the two trends for both
411 periods are generally consistent, but are less so as compared to the entire
412 2005–2013 period. OMI observations suggest a stronger average decrease of
413 5%/yr as compared to 3.7%/yr from AQS data for 2005–2008, whereas the
414 AQS data suggest a larger reduction of 2.8%/yr as compared to 1.6%/yr
415 from OMI data for 2010–2013.

416 There are two main reasons for the change in the pace of reductions.
417 First, emission control devices (ECDs) were installed on many power plants
418 by 2008, reducing their NO_x emissions and, subsequently, the OMI NO_2
419 levels above the facilities dramatically (Duncan et al., 2013). The larger
420 decrease seen in the eastern U.S. resulted from the 2005 Clean Air Interstate
421 Rule (CAIR) for 27 eastern states with the goal to decrease NO_x emissions
422 from power plants. Second, U.S. emissions decreased in 2008 due to the
423 global economic downturn. OMI NO_2 levels changed little in many areas
424 of the country in the latter period as the U.S. economy slowly recovered
425 (Bishop and Stedman, 2014; Tong et al., 2014), but, at the same time, the
426 fleet of light-duty vehicles continued to become more fuel efficient and less
427 polluting (e.g. Bishop and Stedman, 2008; Russell et al., 2012) to meet the
428 more stringent Tier 2 standards of the Clean Air Act Amendments of 1990.

429 *3.4. OMI NO_2 trends over major U.S. metro areas and power plants*

430 In this section, we present the reductions in OMI NO_2 VCDs for 20 U.S.
431 metropolitan areas and over 150 of the largest U.S. power plants.

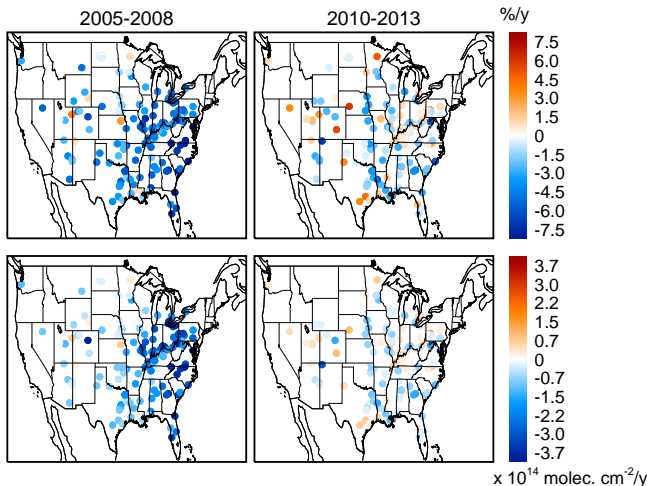


Figure 9: Relative (top) and absolute (bottom) annual trend in OMI tropospheric NO₂ VCDs for 2005–2008 (left) and 2010–2013 (right) over 150 high-emitting U.S. power plants.

432 *3.4.1. Trends over 20 metropolitan areas*

433 As shown in Figures 6 and 8, the largest percent decreases occurred in
 434 heavily populated, urban areas, which are collocated with the highest emis-
 435 sions. Table 4 shows the total reduction (%) in OMI NO₂ levels for 20
 436 metropolitan areas for the period, 2005 to 2013, and the annual trends (%/yr)
 437 for the two sub-periods discussed in the previous section. Levels decreased
 438 by > 40 % in 8 of the 20 cities, including New York City, Los Angeles, and
 439 Philadelphia, 30–40 % in 6 cities, and 20–30 % in 6 cities. In all cities, the
 440 major decrease in levels occurred in the earlier period, 2005–2008, with small
 441 or insignificant changes in the latter period, 2010–2013.

442 *3.4.2. Trends over 150 power plants*

443 Over the OMI record, 2005–2013, U.S. NO_x emissions from power plants
 444 decreased by about 52 % (<http://www.epa.gov/ttn/chief/trends/index>).

Table 4: Annual Average OMI Tropospheric NO₂ VCD in 2005 and 2013, Total Reduction (%) for 2005–2013, and Annual Trend (%/yr) for 20 U.S. Metropolitan Areas.

Cities	Tropospheric NO ₂ VCD		2005–2013 reduction (%)	Annual trend	
	(10 ¹⁵ molec. cm ⁻²)			(%/yr)	
	2005	2013		2005–2008	2010–2013
New York	16.5	11.2	40.9	-6.7	1.3
Los Angeles	20.5	11.8	43.6	-4.3	-4.3
Chicago	10.8	8.8	29.7	-2.6	-1.0
Dallas	5.7	3.8	38.5	-4.1	-2.0
Houston	8.5	5.2	39.4	-7.9	0.9
Philadelphia	10.9	6.7	47.1	-5.2	-0.4
Washington DC	9.6	4.7	48.6	-6.7	-3.4
Miami	4.3	3.3	23.0	-6.4	0.5
Atlanta	9.2	4.5	46.6	-7.9	-2.2
Boston	7.1	5.0	35.7	-8.1	-0.3
San Francisco	5.0	4.0	30.2	-2.3	-1.8
Phoenix	6.8	4.0	46.6	-6.7	-0.8
Detroit	9.4	5.2	25.1	-3.1	-1.3
Seattle	5.7	3.9	25.5	-2.9	-0.6
Minneapolis	4.9	3.1	23.4	-2.8	-1.9
San Diego	5.8	3.9	36.2	-5.0	-3.3
Tampa	5.0	2.8	47.0	-6.6	0.2
St. Louis	5.8	3.9	31.5	-5.0	0.6
Baltimore	8.6	5.4	40.2	-5.5	-1.5
Denver	7.0	5.6	26.3	-4.9	-2.8

445 [html](#)). Duncan et al. (2013) found that changes in OMI NO₂ levels near
446 55 power plants are consistent with changes in each facility's emissions as
447 reported to the CEMS and that the implementation of ECDs was clear in
448 the OMI data for the majority of facilities. Figure 9 shows the annual change
449 (%/yr) in OMI NO₂ levels over 150 of the largest power plants in the U.S. The
450 largest decreases occurred in the eastern U.S. and by 2008, which is consistent
451 with compliance with the provisions of the CAIR. On average, OMI NO₂
452 levels decreased by 4.0 %/yr during the 2005–2008 period and by 0.6 %/yr
453 during the 2010–2013 period. The number of power plants exhibiting positive
454 trends increased from 10 during 2005–2008 to 59 during 2010–2013, although
455 the trends are either small or insignificant (Figure 9).

456 **4. Discussion and conclusions**

457 Satellite data are currently being used in many air quality applications
458 (e.g., Duncan et al., 2014) and uniquely have the advantage of spatial cover-
459 age as compared to sparse surface networks. While the satellite data do not
460 currently provide nose-level concentrations, they are of sufficient maturity
461 that they do deliver important quantitative information on the trends and
462 variations in pollutants important to the air quality community. For instance,
463 Duncan et al. (2013) showed that trends and variations in OMI NO₂ data
464 above U.S. power plants agree well with trends and variations in their emis-
465 sions reported to CEMS, particularly for large facilities. In this manuscript,
466 we show the good correspondence of trends and variations in OMI NO₂ VCD
467 data to another common air quality quantity, surface concentration from the
468 EPA AQS network of surface air quality monitors.

469 Linear trends (2005–2013), estimated from OMI NO₂ VCD data, com-
470 pare well with those from AQS data when grouped by region, land use, and
471 land type. We found that there are an insufficient number of surface NO₂
472 monitors (e.g., 0–2) in most cities to estimate an overall trend in a given
473 metropolitan area. The under-representativeness of an individual monitor
474 for a metropolitan region is highly dependent on site location, particularly
475 those located near major pollution sources (e.g., highways). Nevertheless,
476 the reductions (2005–2013) estimated from AQS data compare favorably for
477 most metropolitan areas as discussed below.

478 Several issues need to be considered when comparing trends and spatial
479 and temporal variations estimated from OMI NO₂ VCD data to those es-
480 timated from surface data. The VCD data are influenced by NO₂ levels in
481 the free troposphere and the relatively coarse spatial resolution of the data
482 may not allow for the VCD data to reflect the variations and trends near
483 individual surface stations, particularly for those stations sited near major
484 pollution sources. However, the satellite data provide greater spatial cov-
485 erage as compared to the relative sparse monitoring network. In addition,
486 AQS monitors measure species other than NO₂, such as some fraction of NO_z
487 (= HNO₃ + PAN + alkyl nitrates), where the NO_z composition is typically
488 unknown. Comparison of the trends inferred from collocated photolytic and
489 molybdenum converter measurements suggests that the true NO₂ trends are
490 likely greater than those computed from AQS data.

491 Despite the limitations of both satellite and surface data, they comple-
492 ment each other and the correlation of the variations in the datasets is rela-
493 tively high for some metropolitan areas. For example, Figure 10 shows the

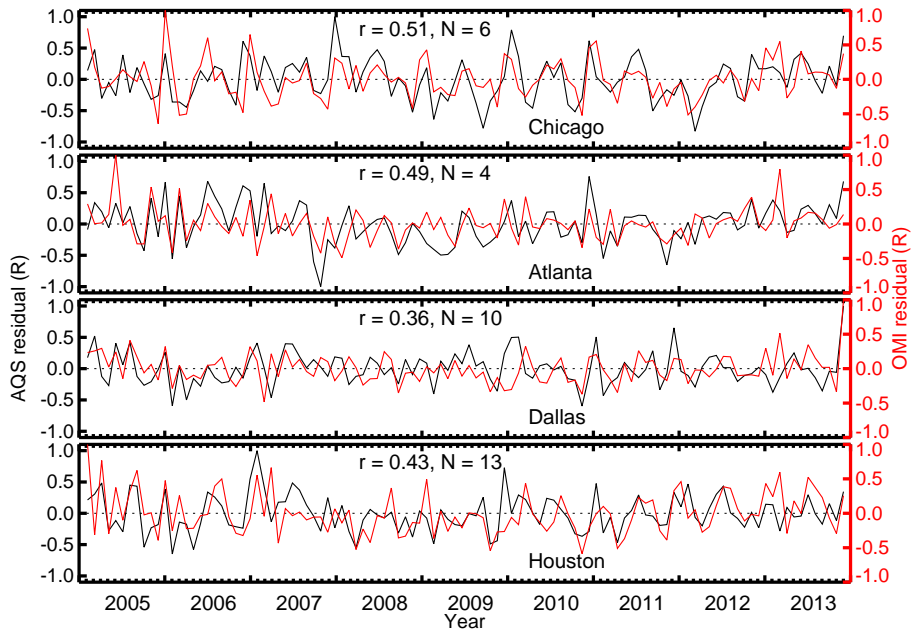


Figure 10: The normalized residual term, R , from Eq. 1 for four U.S. metropolitan areas. The correlation coefficients (r) and number of AQS monitors (N) are given for each city. The OMI data are sampled at the same locations as the AQS data.

494 normalized residual term, R , from Eq. 1. R reflects variations between the
 495 two datasets not explained by the seasonal cycle (α) nor the linear trend
 496 (β) regression terms. It incorporates fluctuations in NO_2 associated with
 497 month-to-month variations in weather, but it also includes variations asso-
 498 ciated with the limitations of the two datasets (e.g., NO_z interferences for
 499 AQS data). We will continue to work to understand the sources of some of
 500 the stronger deviations in R between the two datasets, such as those that
 501 occurred in late 2009 in both Houston and Dallas (Figure 10).

502 In addition to understanding the sources of differences between the two
 503 datasets, work is ongoing to further refine and tailor the OMI NO_2 retrieval

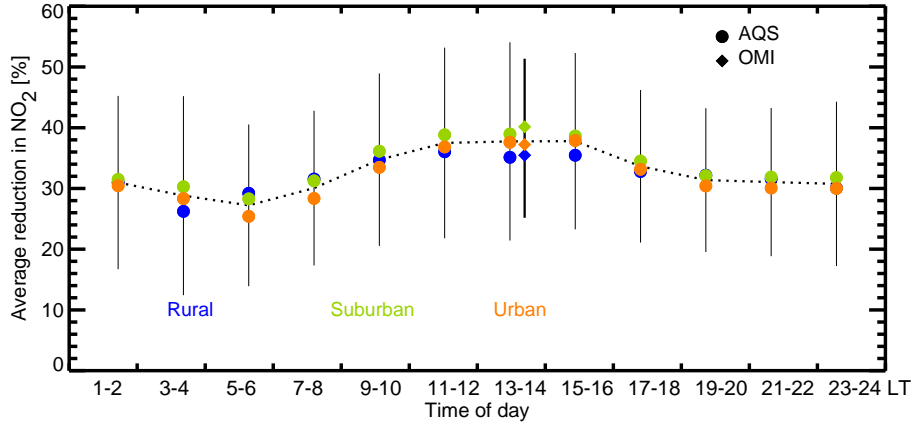


Figure 11: Diurnal changes in NO₂ reductions calculated from 2-hour average NO₂ mixing ratios (circles) in rural (blue), suburban (green), and urban (orange) EPA AQS sites. Dotted line represents average value for all land types. Values shown are the reductions from 2005 to 2013. Diamonds represent reductions in OMI tropospheric NO₂ VCDs. The bars represent the 1 σ variability of the average.

504 algorithm for air quality applications. In this manuscript, for instance, we
 505 showed that, by capturing the general trend in the vertical profile of NO₂ con-
 506 centrations, the comparison between the satellite and surface data improves,
 507 particularly in less polluted areas. Our ongoing retrieval algorithm develop-
 508 ment consists of improved retrievals of SCDs (Marchenko et al., 2014), use
 509 of high-resolution MODIS surface reflectivity together with explicit aerosol
 510 corrections in the AMF calculation, and coupled NO₂ and cloud retrievals,
 511 and these improvements should improve the quality of OMI NO₂ data and
 512 their scientific applications.

513 As a final comment, the Aura satellite overpasses a given location once
 514 a day in early afternoon local time, which limits the data's usefulness, such
 515 as for estimating the diurnal variation of emissions from mobile and point

516 sources. Concentrations of NO_2 in urban areas undergo strong diurnal vari-
517 ations with higher values during the night when photolysis ceases to convert
518 NO_2 to NO , a trace gas that is a member of the NO_x family that cannot
519 be measured from space, and the boundary layer height shrinks, trapping
520 fresh NO_x emissions near the surface, particularly in early morning during
521 rushhour. For our purpose of estimating NO_2 trends, we found that there is
522 little variation in the reductions estimated from AQS data during daylight
523 hours and the reductions estimated from OMI data. Figure 11 indicates
524 that the reductions during the night are generally lower than during the day
525 (i.e., 27 % at 5–6 AM to 38 % at 3–4 PM), which should be considered when
526 inferring changes in emissions, such as mobile sources, from the OMI data.

527 There are two upcoming satellite missions that are relevant for air quality
528 applications using NO_2 VCD data, including the application presented in this
529 manuscript. Both instruments will provide data similar to the OMI, but with
530 improved capabilities. The NASA Tropospheric Emissions: Monitoring of
531 Pollution (TEMPO) instrument (Chance et al., 2013) will be in geostationary
532 orbit, continuously observing the U.S. during daylight hours; the satellite's
533 orbital period will match the Earth's rotational period, so the satellite will
534 appear to be motionless to an observer on the Earth's surface. This orbit will
535 improve the signal-to-noise ratio of the data and allow for the estimation of
536 NO_2 trends and emissions throughout the day. The European Space Agency's
537 (ESA) Tropospheric Ozone Monitoring Instrument (TROPOMI, (Veefkind
538 et al., 2012)) will be launched in 2016 and have a similar once daily overpass
539 time as OMI, but its pixels will have finer spatial resolution, which will
540 allow for better detection of smaller emissions sources and likely improve the

541 comparison of trends and variations with AQS data.

542 **AppendixA. Graphical illustration of the multivariate regression** 543 **analysis**

544 Figure A1 illustrates the variation of the four subcomponents with time
545 from OMI tropospheric NO₂ columns over the eastern U.S. In this example,
546 seasonal variation and linear trend contribute, respectively, 74 % and 11 % of
547 the total variance. The residual contains the impact of short-term variations
548 (e.g. transport) in NO₂ columns that were not captured by the regression
549 model, and represents about 12 % of the total variance. The original and
550 modeled time series constructed from seasonal and trend components are
551 highly correlated ($r = 0.92$, $N = 108$), suggesting that the approach offers a
552 simple yet robust seasonal and trend estimates.

553 **AppendixB. The GMI model**

554 The GMI CTM is driven by meteorology from the Modern Era Retrospective-
555 Analysis for Research and Applications (MERRA) (Rienecker et al., 2011),
556 which reasonably reproduces observed weather for the Aura record (2005–
557 2013). The simulation is performed at 1° latitude × 1.25° longitude horizon-
558 tal resolution and with 72 vertical levels extending from the surface to 0.01
559 hPa. About 33 levels are in the troposphere, including 8 levels below 1 km.
560 The model output is sampled at the OMI overpass time for a self-consistent
561 comparison with the observational dataset.

562 We use a simulation for 2005–2010 that uses monthly and annually vary-
563 ing emissions of CO, NO_x, and non-methane hydrocarbons. Anthropogenic

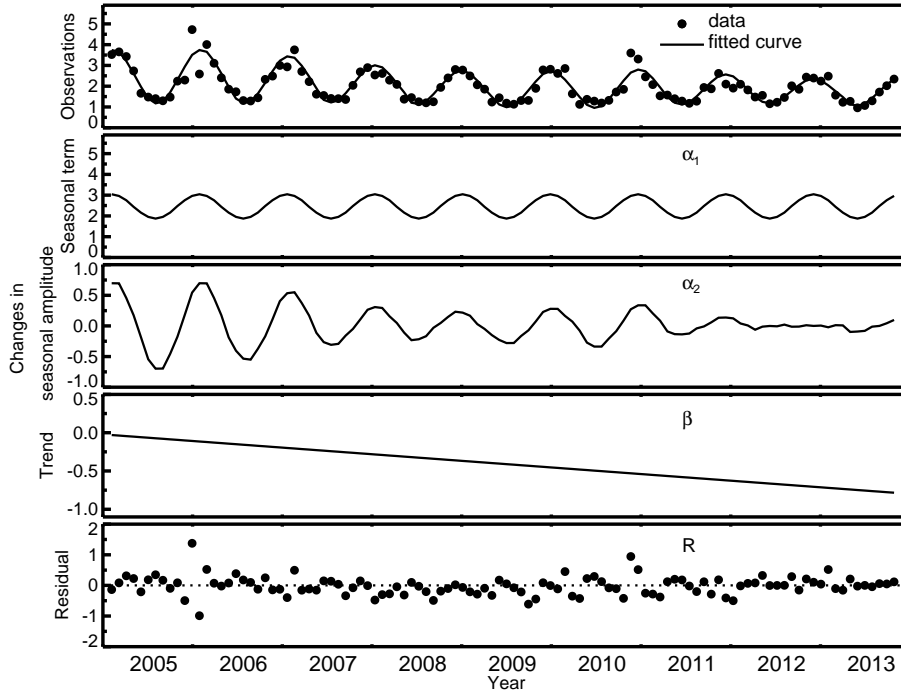


Figure A1: Time series of monthly OMI tropospheric NO_2 columns (Ω , 10^{15} molecules cm^{-2}) over the eastern U.S. ($36\text{--}40^\circ\text{N}$, $70\text{--}75^\circ\text{W}$) separated into four subcomponents: seasonal cycle and change in seasonal amplitude ($\alpha = \alpha_1 + \alpha_2$), long-term linear trend (β), and residuals (R). The line in the top row represents the summation of the α and β subcomponents, and the filled circles represent the actual OMI data.

564 emissions are based on the EDGAR3.2 Inventory (Olivier et al., 2005), over-
565 written by regional inventories: The EPA NEI 2005 inventory ([http://www.
566 epa.gov/ttnchie1/net/2005inventory.html](http://www.epa.gov/ttnchie1/net/2005inventory.html)) over the U.S., CAC ([https:
567 //www.ec.gc.ca](https://www.ec.gc.ca)) over Canada, BRAVO over Mexico (Kuhns et al., 2005),
568 the European Monitoring and Evaluation Programme (EMEP, [http://www.
569 emep.int](http://www.emep.int)) over Europe, and inventory from Zhang et al. (2009) over Asia.
570 The anthropogenic emissions prior to 2006 are scaled applying annual scaling
571 factors from the GEOS-Chem model (van Donkelaar et al., 2008). For 2007–
572 2010, the U.S. and European emissions are scaled on a country-wide basis
573 using the national emission totals from EPA and EMEP, respectively. The
574 REAS inventory projections (Ohara et al., 2007) are used to scale the Asian
575 anthropogenic emissions for 2007–2009. Soil NO_x emissions are computed
576 online with temperature and precipitation dependence ((Yienger and Levy,
577 1995). Lightning NO_x emissions are calculated following Allen et al. (2010).

578 **AppendixC. Details of the OMI retrieval algorithm**

579 We use the OMI standard product, OMNO2 (version 2.1), which is pub-
580 licly available from the NASA Goddard Earth Sciences Data Active Archive
581 Center (GES DISC, <http://disc.sci.gsfc.nasa.gov>). This data version
582 includes significant updates and improvements over previous versions (Buc-
583 sela et al., 2006; Celarier et al., 2008; Lamsal et al., 2008, 2010). Detailed
584 descriptions of the current algorithm and assessments for the standard OMI
585 NO₂ product are given in Bucsela et al. (2013) and Lamsal et al. (2014),
586 respectively. In brief, the algorithm retrieves NO₂ slant column densities
587 (SCDs) with the Differential Optical Absorption Spectroscopy (DOAS) tech-

588 nique (Platt, 1994) in the visible region (405–465 nm). This is followed by
589 computation of air mass factors (AMFs) by integrating relative vertical dis-
590 tribution (shape factors) of NO₂ weighted by altitude dependent scattering
591 weight factors. The NO₂ vertical profiles are simulated by the GMI CTM
592 (Strahan et al., 2007; Duncan et al., 2007) at 2° latitude × 2.5° longitude hor-
593 izontal resolution for the time of the OMI measurement. Scattering weights
594 are computed as a function of reflectivity and pressure of cloud and terrain,
595 and viewing geometry with a radiative transfer model. Stratospheric AMFs
596 and retrieved SCDs from five consecutive orbits over clean regions (30°S–5°N)
597 are used to correct for cross-track biases (stripes) in SCDs resulting from cal-
598 ibration errors. Stratospheric NO₂ fields needed to derive tropospheric NO₂
599 VCDs are determined by box-car smoothing and interpolation of OMI NO₂
600 VCDs estimates, after accounting for a priori tropospheric NO₂ VCDs over
601 unpolluted or cloudy areas. Comparison of OMI tropospheric NO₂ VCDs
602 with a suite of in situ and remote sensing measurements suggests agreement
603 within ± 20 % for clear-sky conditions (Lamsal et al., 2014).

604 **Acknowledgements**

605 The work was supported by the NASA Air Quality Applied Science Team
606 (AQAST) and NASA’s Earth Science Directorate Atmospheric Composition
607 Programs.

608 **References**

609 Allen, D., Pickering, K., Duncan, B., Damon, M., 2010. Impact of light-
610 ning no emissions on north american photochemistry as determined us-

611 ing the global modeling initiative (gmi) model. *J. Geophys. Res.* 115,
612 doi:10.1029/2010jd014062.

613 Beirle, S., Platt, U., Wenig, M., Wagner, T., 2003. Weekly cycle of NO₂
614 by GOME measurements: a signature of anthropogenic sources. *Atmos.*
615 *Chem. Phys.* 3, 2225–2232.

616 Bishop, G. A., Stedman, D. H., 2008. A decade of on-road emissions mea-
617 surements. *Environ. Sci. Technol.* 42, 1651–1656, DOI: 10.1021/es702413b.

618 Bishop, G. A., Stedman, D. H., 2014. The recession of 2008 and its impact on
619 light-duty vehicle emissions in three western United States cities. *Environ.*
620 *Sci. Technol.* 48, 14822–14827, DOI: 10.1021/es5043518.

621 Boersma, K. F., Eskes, H. J., Brinkma, E. J., 2004. Error analy-
622 sis for tropospheric NO₂ retrieval from space. *J. Geophys. Res.* 109,
623 doi:10.1029/2003JD003962.

624 Boersma, K. F., Eskes, H. J., Dirksen, R. J., van der A, R. J., Veefkind,
625 J. P., et al., 2011. An improved tropospheric no₂ column retrieval algorithm
626 for the ozone monitoring instrument. *Atmos. Meas. Tech.* 4, 1905–1928,
627 doi:10.5194/amt-4-1905-2011.

628 Boersma, K. F., Jacob, D. J., Bucsela, E. J., Perring, A. E., Dirksen, R., van
629 der A, R. J., Yantosca, R. M., Park, R. J., Wenig, M. O., Bertram, T. H.,
630 Cohen, R. C., 2008a. Validation of OMI tropospheric NO₂ observations
631 during INTEX-B and application to constrain NO_x emissions over the
632 eastern United States and Mexico. *Atmos. Environ.* 42, 4480–4497.

633 Boersma, K. F., Jacob, D. J., Eskes, H. J., Pinder, R. W., Wang, J., van der
634 A, R. J., 2008b. Intercomparison of SCIAMACHY and OMI tropospheric
635 NO₂ columns: observing the diurnal evolution of chemistry and emissions
636 from space. *J. Geophys. Res.* 113, doi:10.1029/2007JD008816.

637 Bucsela, E. J., Celarier, E. A., Wenig, M. O., Gleason, J. F., Veefkind, J. P.,
638 Boersma, K. F., Brinksma, E. J., 2006. Algorithm for NO₂ vertical column
639 retrieval from the Ozone Monitoring Instrument. *IEEE Trans. Geo. Rem.*
640 *Sens.* 44, 1245–1258.

641 Bucsela, E. J., Krotkov, N. A., Celarier, E. A., Lamsal, L. N., Swartz, W. H.,
642 Bhartia, P. K., Boersma, K. F., Veefkind, J. P., Gleason, J. F., Pickering,
643 K. E., 2013. A new stratospheric and tropospheric NO₂ retrieval algorithm
644 for nadir-viewing satellite instruments: application to OMI. *Atmos. Meas.*
645 *Tech.* 6, 2607–2626.

646 Castellanos, P., Boersma, K. F., 2012. Reductions in nitrogen oxides over
647 Europe driven by environmental policy and economic recession. *Sci. Rep.*
648 2, 2, 265, DOI:10.1038/srep00265.

649 Celarier, E. A., Brinksma, E. J., Gleason, J. F., Veefkind, J. P., Cede, A.,
650 Herman, J. R., Ionov, D., Goutail, F., Pommereau, J. P., Lambert, J. C.,
651 van Roozendaal, M., Pinardi, G., Witrock, F., Schönhardt, A., Richter,
652 A., Ibrahim, O. W., Wagner, T., Bojkov, B., Mount, G., Spinei, E., Chen,
653 C. M., Pongetti, T. J., Sander, S. P., Bucsela, E. J., Wenig, M. O., Swart,
654 D. P. J., Volten, H., Kroon, M., Levelt, P. F., 2008. Validation of Ozone
655 Monitoring Instrument nitrogen dioxide columns. *J. Geophys. Res.* 113,
656 doi:10.1029/2007JD008908.

657 Challen, P., Hickish, D., Bedford, J., 1958. An investigation of some health
658 hazards in an inert-gas tungsten-arc welding shop. *Br. J. Ind. Med.* 15,
659 276–282.

660 Chance, K., Liu, X., Suleiman, R. M., Flittner, D. E., Al-Saadi, J., Janz,
661 S. J., 2013. *Tropospheric emissions: Monitoring of pollution (TEMPO)*.
662 SPIE Publication, 8866–11.

663 Cleveland, R. B., Cleveland, W. S., McRae, J. E., Terpenning, I., 1990. STL:
664 A seasonal-trend decomposition procedure based on Loess. *J. Off. Stat.* 6,
665 1, 3–33.

666 Demerjian, K. L., 2000. A review of national monitoring networks in North
667 America. *Atmos. Environ.* 34, 1861–1884.

668 Duncan, B. N., Chameides, W., 1998. The effects of urban emission control
669 strategies on the export of ozone and ozone precursors from the urban
670 atmosphere to the troposphere. *J. Geophys. Res.* 103, 28,159–28179.

671 Duncan, B. N., Prados, A. I., Lamsal, L. N., Liu, Y., Streets, D., Gupta,
672 P., Hilsenrath, E., Kahn, R., Nielsen, J. E., Beyersdorf, A., Burton, S.,
673 Fiore, A. M., Fishman, J., Henze, D., Hostetler, C., Krotkov, N. A., Lee,
674 P., Lin, M., Pawson, S., Pfister, G., Pickering, K. E., Pierce, B., Yoshida,
675 Y., Ziemba, L., 2014. *Satellite data of atmospheric pollution for U.S. air
676 quality applications: Examples of applications, summary of data end-user
677 resources, answers to FAQs, and common mistakes to avoid.* *Atmos. Env-
678 iron.* 94.

679 Duncan, B. N., Strahan, S. E., Yoshida, Y., Steenrod, S. D., Livesey, N.,
680 2007. Model study of the cross-tropopause transport of biomass burning
681 pollution. *Atmos. Chem. Phys.* 7, 3713–3736.

682 Duncan, B. N., Yoshida, Y., de Foy, B., Lamsal, L. N., Streets, D., Lu, Z.,
683 Pickering, K. E., Krotkov, N. A., 2013. The observed response of the Ozone
684 Monitoring Instrument (OMI) NO₂ column to NO_x emission controls on
685 power plants in the United States: 2005-2011. *Atmos. Environ.* 81, 102–
686 111.

687 Duncan, B. N., Yoshida, Y., Olson, J., Sillman, S., Martin, R. V., Lamsal,
688 L. N., Hu, Y., Pickering, K., Retscher, C., Allen, D., Crawford, J., 2010.
689 Application of OMI observations to a space-based indicator of NO_x and
690 VOC controls on surface ozone formation. *Atmos. Environ.* 44, 2213–2223.

691 Dunlea, E. J., Herndon, S. C., Nelson, D. D., Volkamer, R. M., San Martini,
692 F., Sheehy, P. M., Zahniser, M. S., Shorter, J. H., Wormhoudt, J., Lamb,
693 B. K., Allwine, E. J., Gaffney, J. S., Marley, N. A., Grutter, M., Marquez,
694 C., Blanco, S., Cardenas, B., Retama, A., Ramos Villegas, C. R., Kolb,
695 C. E., Molina, L. T., Molina, M. J., 2007. Evaluation of nitrogen diox-
696 ide chemiluminescence monitors in a polluted urban environment. *Atmos.*
697 *Chem. Phys.* 7, 2691–2704.

698 Edgerton, E. S., Hartsell, B. E., Saylor, R. D., Jansen, J. J., Hansen, D. A.,
699 Hidy, G. M., 2006. The Southeastern Aerosol Research and Characteriza-
700 tion Study, part 3: Continuous measurements of fine particulate matter
701 mass and composition. *J. Air Waste Mgt. Assoc.* 56(9), 1325–1341.

702 EPA, 1975. Technical assistance document for the chemiluminescence mea-
703 surement of nitrogen dioxide, tech. rep.,. Tech. rep., U.S. Environmental
704 Protection Agency, Research Triangle Park, NC 27711, EPA-600/4-75-003.

705 EPA, 2006. Air quality criteria for ozone and related photochemical oxi-
706 dants. Tech. rep., U.S. Environmental Protection Agency, Research Trian-
707 gle Park,NC 27711, EPA 454/K-01-002.

708 EPA, 2008. Integrated science assessment for oxides of nitrogen - health crite-
709 ria (first external review draft). Tech. rep., U.S. Environmental Protection
710 Agency, Research Triangle Park,NC 27711, EPA/600/R-07/093.

711 EPA, 2012. Our nation's air: Status and trends through 2010. Tech. rep.,
712 Environmental Protection Agency, EPA-454/R-12001.

713 Frost, G. J., McKeen, S. A., Trainer, M., Ryerson, T. B., Neuman, J. A.,
714 Roberts, J. M., Swanson, A., Holloway, J. S., Sueper, D. T., Fortin, T.,
715 Parrish, D. D., Fehsenfeld, F., Flocke, F., Peckham, S. E., Grell, G. A.,
716 Kowal, D., Cartwright, J., Auerbach, N., Habermann, T., 2006. Effects of
717 changing power plant NO_x emissions on ozone in the eastern United States:
718 Proof of concept. *J. Geophys. Res.* 111, doi:10.1029/2005JD006354.

719 Ghude, S. D., Pfister, G. G., Jena, C., et al., 2013. Satellite constraints of
720 nitrogen oxide emissions from India based on OMI observations and WRF-
721 Chem simulations. *Geophys. Res. Lett.* 40, doi:10.1029/2012GL053926.

722 Grosjean, D., Harrison, J., 1985. Response of chemiluminescence NO_x ana-
723 lyzers and ultraviolet ozone analyzers to organic air pollutants. *Environ.*
724 *Sci. Technol.* 19, 862–865.

- 725 Hains, J., Boersma, K. F., Kroon, M., et al., 2010. Testing and improving
726 OMI DOMINO tropospheric NO₂ using observations from the DANDE-
727 LIONS and INTEX-B validation campaigns. *J. Geophys. Res.* 115, D05301,
728 doi:10.1029/2009JD012399.
- 729 Heckel, A., Kim, S. W., Frost, G. J., Richter, A., Trainer, M., Burrows, J. P.,
730 2011. Influence of low spatial resolution a priori data on tropospheric NO₂
731 satellite retrievals. *Atmos. Meas. Tech.* 4(9), 1805–1820, doi:10.5194/amt-
732 4-1805-2011.
- 733 Hilboll, A., Richter, A., Burrows, J. P., 2013. Long-term changes of tropo-
734 spheric NO₂ over megacities derived from multiple satellite instruments.
735 *Atmos. Chem. Phys.* 13, 4145–4169, doi:10.5194/acp-13-4145-2013.
- 736 Jaeglé, L., Steinberger, L., Martin, R. V., Chance, K., 2005. Global parti-
737 tioning of NO_x sources using satellite observations: Relative roles of fossil
738 fuel combustion, biomass burning and soil emissions. *Faraday Discussions*
739 130, doi: 10.1039/b502128f.
- 740 Kim, S. W., Heckel, A., McKeen, S. A., Frost, G. J., Hsie, E. Y.,
741 Trainer, M. K., Richter, A., Burrows, J. P., Peckham, S. E., Grell,
742 G. A., 2006. Satellite-observed U.S. power plant NO_x emission reduc-
743 tions and their impact on air quality. *Geophys. Res. Lett.* 33, L22812,
744 doi:10.1029/2006GL027749.
- 745 Kleinfeld, M., Giel, C., Tabershaw, I., 1957. Health hazards associated with
746 inert gas shield metal arc welding. *Arch. Ind. Health* 15, 27–31.

- 747 Kley, D., McFarland, M., 1980. Chemiluminescence detector for NO and
748 NO₂. *Atmos. Tech.* 12, 63–69.
- 749 Kuhns, H., Knipping, E. M., Vokovich, J. M., 2005. Development of a United
750 States-Mexico emissions inventory for the Big Bend Regional Aerosol and
751 Visibility Observational (BRAVO) study. *J. Air Waste Mgt. Assoc.* 55,
752 677–692.
- 753 Lamsal, L. N., Krotkov, N. A., Celarier, E. A., Swartz, W. H., Pickering,
754 K. E., Bucsela, E. J., Gleason, J. F., Martin, R. V., Philip, S., Irie, H.,
755 Cede, A., Herman, J., Weinheimer, A., Szykman, J. J., Knepp, T. N., 2014.
756 Evaluation of OMI operational standard no₂ column retrievals using in situ
757 and surface-based no₂ observations. *Atmos. Chem. Phys.* 14, 11587-11609,
758 doi:10.5194/acp-14-11587-2014.
- 759 Lamsal, L. N., Martin, R. V., Padmanabhan, A., van Donkelaar, A., Zhang,
760 Q., Sioris, C. E., Chance, K., Kurosu, T. P., Newchurch, M. J., 2011.
761 Application of satellite observations for timely updates to global an-
762 thropogenic NO_x emission inventories. *Geophys. Res. Lett.* 38, L05810,
763 doi:10.1029/2010GL046476.
- 764 Lamsal, L. N., Martin, R. V., van Donkelaar, A., Celarier, E. A., Bucsela,
765 E. J., Boersma, K. F., Luo, R. D. C., Wang, Y., 2010. Indirect validation
766 of tropospheric nitrogen dioxide retrieved from the OMI satellite instru-
767 ment: Insight into the seasonal variation of nitrogen oxides at northern
768 midlatitudes. *J. Geophys. Res.* 115, D05302, doi:10.1029/2009JD013351.
- 769 Lamsal, L. N., Martin, R. V., van Donkelaar, A., Steinbacher, M., Celarier,

- 770 E. A., Bucselá, E., Dunlea, E. J., Pinto, J. P., 2008. Ground-level nitrogen
771 dioxide concentrations inferred from the satellite-borne Ozone Monitoring
772 Instrument. *J. Geophys. Res.* 113, D16308, doi:10.1029/2007JD009235.
- 773 Leue, C., Wenig, M., Wagner, T., Klimm, O., Platt, U., Jähne, B., 2001.
774 Quantitative analysis of NO₂ emissions from Global Ozone Monitoring
775 Experiment satellite image sequences. *J. Geophys. Res.* 106, 5493–5505.
- 776 Lin, J. T., McElroy, M. B., 2011. Detection from space of a reduction in
777 anthropogenic emissions of nitrogen oxides during the Chinese economic
778 downturn. *Atmos. Chem. Phys.* 11, 8171–8188, doi:10.5194/acp-11-8171-
779 2011.
- 780 Lin, J. T., McElroy, M. B., Boersma, K. F., 2010. Constraint of anthro-
781 pogenic NO_x emissions in China from different sectors: a new methodology
782 using multiple satellite retrievals. *Atmos. Chem. Phys.* 10, 63–78.
- 783 Marchenko, S., Krotkov, N. A., Lamsal, L. N., Celarier, E. A., Swartz, W. H.,
784 Bucselá, E. J., 2014. Towards a more accurate slant column density re-
785 trieval of nitrogen dioxide from space. *J. Geophys. Res.* TBD, submitted.
- 786 Martin, R. V., Chance, K., Jacob, D. J., et al., 2002. An improved re-
787 trieval of tropospheric nitrogen dioxide from GOME. *J. Geophys. Res.*
788 107, doi:10.1029/2001JD001027.
- 789 Martin, R. V., Jacob, D. J., Chance, K., Kurosu, T. P., Perner, P. I.,
790 Evans, M. J., 2003. Global inventory of nitrogen oxide emission con-
791 strained by space-based observations of NO₂ columns. *J. Geophys. Res.*
792 108, doi:10.1029/2003JD003453.

- 793 Martin, R. V., Parrish, D. D., Ryerson, T. B., Jr., D. K. N., Chance, K.,
794 Kurosu, T. P., Jacob, D. J., Sturges, E. D., Fried, A., Wert, B. P., 2004.
795 Evaluation of GOME satellite measurements of tropospheric NO₂ and
796 HCHO using regional data from aircraft campaigns in the southeastern
797 United States. *J. Geophys. Res.* 109, doi:10.1029/2004JD004869.
- 798 McDonald, B. C., Dallmann, T. R., Martin, E. W., Harley, R. A., 2012.
799 Long-term trends in nitrogen oxide emissions from motor vehicles at
800 national, state, and air basin scales. *J. Geophys. Res.* 117, D00V18,
801 doi:10.1029/2012JD018304.
- 802 Napelenok, S. L., Pinder, R. W., Gilliland, A. B., Martin, R. V., 2008. A
803 method for evaluating spatially-resolved NO_x emissions using Kalman filter
804 inversion, direct sensitivities, and space-based NO₂ observations. *Atmos.*
805 *Chem. Phys.* 8, 5603–5614.
- 806 Ohara, T., Akimoto, H., Kurokawa, J., Horii, N., Yamaji, K., Yan, X.,
807 Hayasaka, T., 2007. An Asian emission inventory of anthropogenic emis-
808 sion sources for the period 1980–2020. *Atmos. Chem. Phys.* 7, 4419–4444.
- 809 Olivier, J. G., Van Aardenne, J. A., Dentener, F. J., Pagliari, V., Ganzeveld,
810 L. N., Peters, J. A., 2005. Recent trends in global greenhouse gas emissions:
811 regional trends 1970–2000 and spatial distribution of key sources in 2000.
812 *Environ. Sci.* 2(2-3), 81–99.
- 813 Platt, U., 1994. Differential Optical Absorption Spectroscopy (DOAS). In:
814 Sigrist, M. W. (Ed.), *Air Monitoring by Spectroscopic Techniques*. John
815 Wiley, New York, USA, pp. 27–84.

- 816 Pollack, I. B., Lerner, B. M., Ryerson, T. B., 2010. Evaluation of ultraviolet
817 light-emitting diodes for detection of atmospheric NO₂ by photolysis
818 chemiluminescence. *J. Atmos. Chem.* 65, 111–125.
- 819 Randel, W. J., Cobb, J. B., 1994. Coherent variations of monthly mean total
820 ozone and lower stratospheric temperature. *J. Geophys. Res.* 99, 5433–
821 5447, doi:10.1029/93JD03454.
- 822 Richter, A., Burrows, J. P., Nüß, H., Granier, C., Niemeier, U., 2005. Increase
823 in tropospheric nitrogen dioxide levels over China observed from space.
824 *Nature* 437, 129–132.
- 825 Rienecker, M. M., Suarez, M. J., Gelaro, R., Todling, R., Bacmeister, J.,
826 Liu, E., Bosilovich, M. G., Schubert, S. D., Takacs, L., Kim, G. K.,
827 Bloom, S., Chen, J., Collins, D., Conaty, A., da Silva, A., Gu, W.,
828 Joiner, J., Koster, R. D., Lucchesi, R., Molod, A., Owens, T., Pawson,
829 S., Pegion, P., Redder, C. R., Reichle, R., Robertson, F. R., Ruddick,
830 A. G., Sienkiewicz, M., Woollen, J., 2011. MERRA: NASA's Modern-Era
831 Retrospective Analysis for Research and Applications. *J. Clim.* 24, doi:
832 <http://dx.doi.org/10.1175/JCLI-D-11-00015.1>.
- 833 Russell, A. R., Perring, A. E., Valin, L. C., Hudman, R. C., Browne, E. C.,
834 Min, K. E., Wooldridge, P. J., Cohen, R. C., 2011. A high spatial resolution
835 retrieval of NO₂ column densities from OMI: method and evaluation.
836 *Atmos. Chem. Phys.* 11, 8543–8554, doi:10.5194/acp-11-8543-2011.
- 837 Russell, A. R., Valin, L. C., Cohen, R. C., 2012. Trends in OMI NO₂ ob-
838 servations over the United States: effects of emission control technol-

839 ogy and the economic recession. *Atmos. Chem. Phys.* 12, 12197–12209,
840 doi:10.5194/acp-12-12197-2012.

841 Ryerson, T. B., Williams, E. J., Fehsenfeld, F. C., 2000. An efficient pho-
842 tolysis system for fast-response NO₂ measurements. *J. Geophys. Res.* 105,
843 26447–26461.

844 Steinbacher, M., Zellweger, C., Schwarzenbach, B., Bugmann, S., Buchmann,
845 B., Ordóñez, C., Prévôt, A. S. H., Hueglin, C., 2007. Nitrogen oxides mea-
846 surements at rural sites in Switzerland: Bias of conventional measurement
847 techniques. *J. Geophys. Res.* 10.1029/2006JD007971.

848 Strahan, S. E., Duncan, B. N., Hoor, P., 2007. Observationally derived trans-
849 port diagnostics for the lowermost stratosphere and their application to the
850 GMI chemistry and transport model. *Atmos. Chem. Phys.* 7, 2435–2445.

851 Streets, D. G., Carmichael, G. R., de Foy, B., Dickerson, R. R., Duncan,
852 B. N., Edwards, D. P., Haynes, J. A., Henze, D. K., Houyoux, M. R.,
853 Jacob, D. J., Krotkov, N. A., Lamsal, L. N., Liu, Y., Lu, Z., Martin, R. V.,
854 Pfister, G. G., Pinder, R. W., Wecht, K. J., 2013. Emissions estimation
855 from satellite retrievals: A review of current capability. *Atmos. Environ.*
856 77, 1011–1042.

857 Strode, S. A., Rodriguez, J. M., Logan, J. A., Cooper, O. R., Witte,
858 J. C., Lamsal, L. N., Damon, M., Steenrod, S. D., Strahan, S. E., 2014.
859 Trends and variability in surface ozone over the United States. *J. Geophys.*
860 *Res.* Submitted.

- 861 Tang, W., Cohan, D., Lamsal, L. N., Xiao, X., Zhou, W., 2013. Inverse
862 modeling of Texas NO_x emissions using space-based and ground-based NO_2
863 observations. *Atmos. Chem. Phys.* 13, 11005–11018.
- 864 Tang, W., Cohan, D., Pour-Biazar, A., Lamsal, L. N., White, A., Xiao, X.,
865 Zhou, W., Henderson, B. H., Lash, B., 2014. Influence of satellite-derived
866 photolysis rates and NO_x emissions on Texas ozone modeling. *Atmos.*
867 *Chem. Phys. Discuss.* 7, 11415–11437, doi:10.5194/acpd-14-24475-2014.
- 868 Tong, D., Lamsal, L. N., Pan, L., Kim, H., Lee, P., Chai, T., Pickering,
869 K. E., 2014. Long-term NO_x trends over large cities in the United States:
870 Intercomparison of satellite retrievals, ground observations, and emission
871 inventories. *Atmos. Environ.* TBD, submitted.
- 872 Valin, L. C., Russell, A. R., Cohen, R. C., 2013. Variation of OH radical in
873 an urban plume inferred from NO_2 column measurements. *Geophys. Res.*
874 *Lett.* 40, 1856–1860.
- 875 van Donkelaar, A., Martin, R. V., Leaitch, W. R., Macdonald, A. M., Walker,
876 T. W., Streets, D. G., Zhang, Q., Dunlea, E. J., Jimenez, J. L., Dibb,
877 J. E., Huey, L. G., Weber, R., Andreae, M. O., 2008. Analysis of aircraft
878 and satellite measurements from the Intercontinental Chemical Transport
879 Experiment (INTEX-B) to quantify long-range transport of East Asian
880 sulfur to Canada. *Atmos. Chem. Phys.* 8, 2999–3014.
- 881 Veefkind, J. P., Aben, I., McMullan, K., Foerster, H., de Vries, J., Otter,
882 G., Claas, J., Eskes, H. J., de Haan, J. F., Kleipool, Q., van Weele, M.,
883 Hasekamp, O., Hoogeveen, R., Landgraf, J., Snel, R., Tol, P., Ingmann,

- 884 P., Voors, R., Kruizinga, B., Vink, R., Visser, H., Levelt, P. F., 2012.
885 TROPOMI on the ESA Sentinel-5 Precursor: A GMES mission for global
886 observations of the atmospheric composition for climate, air quality and
887 ozone layer applications. *Rem. Sen. Env.* 120, 70–83.
- 888 Vinken, G. C. M., Boersma, K. F., van Donkelaar, A., Zhang, L., 2014.
889 Constraints on ship NO_x emissions in Europe using GEOS-Chem and
890 OMI satellite NO_2 observations. *Atmos. Chem. Phys.* 14, 1353–1369,
891 doi:10.5194/acp-14-1353-2014.
- 892 Wang, S. W., Zhang, Q., Streets, D. G., He, K. B., Martin, R. V., Lamsal,
893 L. N., Chen, D., Lei, Y., Lu, Z., 2012. Growth in NO_x emissions from
894 power plants in China: bottom-up estimates and satellite observations.
895 *Atmos. Chem. Phys.* 12, 4429–4447, doi:10.5194/acp-12-4429-2012.
- 896 Wang, Y. X., McElroy, M. B., Martin, R. V., Streets, D. G., Zhang, Q.,
897 Fu, T.-M., 2007. Seasonal variability of NO_x emissions over east China
898 constrained by satellite observations: Implications for combustion and mi-
899 crobial sources. *J. Geophys. Res.* 112, doi:10.1029/2006JD007538.
- 900 Winer, A. M., Peters, J. W., Smith, J. P., Pitts Jr., J. N., 1974. Response
901 of commercial chemiluminescent NO- NO_2 analyzers to other nitrogen con-
902 taining compounds. *Environ. Sci. Technol.* 8, 1118–1121.
- 903 Xing, J., Pleim, J., Mathur, R., Pouliot, G., Hogrefe, C., Gan, C. M., Wei, C.,
904 2013. Historical gaseous and primary aerosol emissions in the United States
905 from 1990 to 2010. *Atmos. Chem. Phys.* 13, 7531–7549, doi:10.5194/acp-
906 13-7531-2013.

- 907 Yienger, J. J., Levy, H., 1995. Empirical model of global soil biogenic NO_x
908 emissions. *J. Geophys. Res.* 100, 11447–11464.
- 909 Zellweger, C., Ammann, M., Buchmann, B., Hofer, P., Lugauer, M., Rütti-
910 mann, R., Streit, N., Weingartner, E., Baltensperger, U., 2000. Summer-
911 time NO_y speciation at the Jungfraujoeh, 3580 m above sea level, Switzer-
912 land. *J. Geophys. Res.* 105, 6655–6667.
- 913 Zhang, Q., Streets, D. G., Carmichael, G. R., He, K., Huo, H., Kannari, A.,
914 Klimont, Z., Park, I., Reddy, S., Fu, J. S., Chen, D., Duan, L., Lei, Y.,
915 Wang, L., Yao, Z., 2009. Asian emissions in 2006 for the NASA INTEX-B
916 mission. *Atmos. Chem. Phys. Discuss.* 9, 4081–4139.
- 917 Zhao, C., Wang, Y., 2009. Assimilation inversion of NO_2 emissions over
918 east Asia using OMI NO_2 column measurements. *Geophys. Res. Lett.* 36,
919 L06805, doi:10.1029/2008GL037129.
- 920 Zhou, Y., Brunner, D., Hueglin, C., s. Henne, Staehelin, J., 2012. Changes
921 in OMI tropospheric NO_2 columns over Europe from 2004 to 2009 the
922 influence of meteorological variability. *Atmos. Environ.* 46.